Supplemental Information

Supplementary Note 1: The single- and three-band Hubbard Models — The Hamiltonian of the three-band Hubbard model is

$$\begin{aligned} H = (\varepsilon_d - \mu)\sum_{i,\sigma} n^d_{i,\sigma} + (\varepsilon_p - \mu)\sum_{j,\sigma} n^{p_\alpha}_{j,\sigma} + \sum_{\langle i,j\rangle,\sigma} t_{ij}(d^\dagger_{i\sigma}p_{\alpha j\sigma} + p^\dagger_{\alpha j\sigma}d_{i\sigma}) \\ + \sum_{\langle j,j'\rangle,\sigma} t_{jj'}(p^\dagger_{\alpha j\sigma}p_{\alpha' j'\sigma} + p^\dagger_{\alpha' j'\sigma}p_{\alpha j\sigma}) + U_{dd}\sum_i n^d_{i\uparrow}n^d_{i\downarrow} + U_{pp}\sum_j n^{p_\alpha}_{j\uparrow}n^p_{j\downarrow}. \end{aligned} \tag{1}$$

Here, $d^\dagger_{i,\sigma}$ ($d_{i,\sigma}$) creates (annihilates) a spin σ ($=\uparrow,\downarrow$) hole in the copper $d_{x^2-y^2}$ orbital at site i; $p^\dagger_{\alpha j\sigma}$ ($p_{\alpha j\sigma}$) creates (annihilates) a spin σ hole in the oxygen p_α ($\alpha = x, y$) orbital at site j; for nearest neighbor, $j = i \pm \hat{x}/2$ (or $\hat{y}/2$); $n^d_{i\sigma} = d^\dagger_{i\sigma}d_{i\sigma}$ and $n^{p_\alpha}_{j\sigma} = p^\dagger_{\alpha j\sigma}p_{\alpha j\sigma}$ are the number operators; ϵ_d and ϵ_p are the onsite energies of the Cu and O orbitals, respectively; μ is the chemical potential; t_{ij} is the nearest neighbor Cu-O hopping integral; $t_{jj'}$ is the nearest neighbor O-O hopping integral; and U_{dd} and U_{pp} are the on-site Hubbard repulsions on the Cu and O orbitals, respectively. The hopping integrals are parameterized [1] as $t_{ij} = P_{ij}t_{pd}$ and $t_{jj'} = Q_{jj'}t_{pp}$, where $P_{ij} = 1$ for $j = i + \hat{y}/2$ or $j = i - \hat{x}/2$, $P_{ij} = -1$ for $j = i - \hat{y}/2$ or $j = i + \hat{x}/2$ and $Q_{jj'} = 1$ for $j' = j - \hat{x}/2 + \hat{y}/2$ or $j' = j + \hat{x}/2 - \hat{y}/2$, $Q_{jj'} = -1$ for $j' = j + \hat{x}/2 + \hat{y}/2$ or $j' = j - \hat{x}/2 - \hat{y}/2$. Throughout, we adopted (in units of eV): $t_{pd} = 1.13$, $t_{pp} = 0.49$, $U_{dd} = 8.5$, $U_{pp} = 0$, and $\Delta = \varepsilon_p - \varepsilon_d = 3.24$ [1–4], unless otherwise stated. Since we use a hole language, half-filling is defined as hole density $n_h = 1$ and $n_h > 1$ corresponds to hole-doping and $n_h < 1$ corresponds to electron-doping. A finite U_{pp} only leads to small quantitative changes in the pair structure (see Supplementary Figure 4), but worsens the sign problem significantly [1]. Therefore, we keep $U_{pp} = 0$ for this study except for the results presented in Supplementary Figure 4.

The downfolded single-band Hubbard model is

$$H = -\mu\sum_{i\sigma} n_{i\sigma} - \sum_{\langle i,j\rangle\sigma} t_{ij}c^\dagger_{i\sigma}c_{j\sigma} + U\sum_i \left(n_{i\uparrow} - \frac{1}{2}\right)\left(n_{i\downarrow} - \frac{1}{2}\right), \tag{2}$$

where $c^\dagger_{i\sigma}$ ($c_{i\sigma}$) creates (annihilates) an electron with spin σ at site i, $t_{i,j} = t$ and t' for nearest- and next-nearest-neighbor hoping, respectively, and zero otherwise. U is the on-site Hubbard repulsion, and μ is the chemical potential, which is adjusted to fix the electron filling. Throughout, we set $t = 1$, $U = 6t$, and vary t' as indicated in the text.

Supplementary Note 2: Symmetrized eigenvectors of the Bethe-Salpeter equation — To determine the structure of the effective pairing interaction, we solve the Bethe-Salpeter equation in the particle-particle singlet channel

$$-\frac{T}{N_c}\sum_{K,\alpha_1,\ldots,\alpha_4}\Gamma^{c,pp}_{\alpha,\beta,\alpha_1,\alpha_2}(K,K')\bar{\chi}_{\alpha_1,\alpha_2,\alpha_3,\alpha_4}(K')\phi^{R,\nu}_{\alpha_3\alpha_4}(K')=\lambda_\nu\phi^{R,\nu}_{\alpha\beta}(K)\,. \tag{3}$$

Here, $K=(\mathbf{K},\mathrm{i}\omega_n)$, and $\bar{\chi}_{\alpha_1,\alpha_2,\alpha_3,\alpha_4}(\mathbf{K},\mathrm{i}\omega_n)=(N_c/N)\sum_{\mathbf{k}'}[G_{\alpha_1\alpha_3}(\mathbf{K}+\mathbf{k}',\mathrm{i}\omega_n)G_{\alpha_2\alpha_4}(-\mathbf{K}-\mathbf{k}',-\mathrm{i}\omega_n)]$ is the coarse-gained bare particle-particle propagator. The irreducible particle-particle vertex $\Gamma^{c,pp}$ is extracted from the two-particle cluster Green's function $G^{2,c}_{\alpha_1,\alpha_2,\alpha_3,\alpha_4}(K,K')$ with zero center of mass momentum and frequency by inverting the cluster Bethe-Salpeter equation

$$\begin{aligned}G^{2,c}_{\alpha_1,\alpha_2,\alpha_3,\alpha_4}(K,K')&=\bar{G}_{\alpha_1,\alpha_3}(K)\bar{G}_{\alpha_2\alpha_4}(-K)\delta_{K,K'}\\&+\frac{T}{N_c}\sum_{K'',\alpha_1',\ldots,\alpha_4'}\bar{G}_{\alpha_1,\alpha_1'}(K)\bar{G}_{\alpha_2,\alpha_2'}(-K)\Gamma^{c,pp}_{\alpha_1',\alpha_2',\alpha_3',\alpha_4'}(K,K'')G^{2,c}_{\alpha_3',\alpha_4',\alpha_3,\alpha_4}(K'',K')\,.\end{aligned} \tag{4}$$

To remove the ambiguity between left and right eigenvectors of the eigenvalue equation (3), we symmetrize the pairing kernel entering Eq. (3). Using matrix notation in (K,α,β), we first diagonalize the bare particle-particle propagator, $\bar{\chi}^D=U^{-1}\bar{\chi}U$, where χ^D is a diagonal matrix, to introduce the symmetrized BSE

$$-\frac{T}{N_c}U\sqrt{\chi^D}U^{-1}\Gamma^{c,pp}U\sqrt{\chi^D}U^{-1}\phi^\nu=\lambda_\nu\phi^\nu\,. \tag{5}$$

We use the eigenvectors of the symmetrized BSE, $\phi^\nu_{\alpha\beta}(K)$, for the analysis presented in the main text. They are related to the right eigenvectors of the BSE in Eq. (3) by

$$\phi^\nu=U\sqrt{\chi^D}U^{-1}\phi^{R,\nu}\,. \tag{6}$$

Supplementary Note 3: The basis transformation to the molecular L, L' orbitals — The construction of the Zhang-Rice singlet relies on a transformation from the oxygen p_x, p_y orbital basis to bonding and anti-bonding molecular orbitals, denoted here as L and L', respectively. The two basis are related by a unitary transformation [5–7] defined in k-space

$$L_{\mathbf{k}\sigma} = \frac{\mathrm{i}}{\gamma_{\mathbf{k}}} \left[\sin\left(\tfrac{k_x a}{2}\right) \; p_{x\mathbf{k}\sigma} - \sin\left(\tfrac{k_y a}{2}\right) \; p_{y\mathbf{k}\sigma} \right], \tag{7}$$

and

$$L'_{\mathbf{k}\sigma} = -\frac{\mathrm{i}}{\gamma_{\mathbf{k}}} \left[\sin\left(\tfrac{k_y a}{2}\right) \; p_{x\mathbf{k}\sigma} + \sin\left(\tfrac{k_x a}{2}\right) \; p_{y\mathbf{k}\sigma} \right], \tag{8}$$

where $\gamma_{\mathbf{k}}^2 = \sin^2(k_x a/2) + \sin^2(k_y a/2)$, $p_{\alpha\mathbf{k}\sigma} = N_c^{-1/2} \sum_j p_{\alpha j\sigma} \exp(-\mathrm{i}\mathbf{k}\cdot\mathbf{R}_j)$, and we have set the lattice constant $a = 1$. In this basis, only the L state hybridizes with the Cu-d orbital, while the L' state only hybridizes with the L state. The Fourier transform of the L and L' orbitals to real-space is defined as $L_{i\sigma} = N^{-1/2} \sum_{\mathbf{k}} L_{\mathbf{k}\sigma} \exp(-\mathrm{i}\mathbf{k}\cdot\mathbf{R}_i)$, $L'_{i'\sigma} = N^{-1/2} \sum_{\mathbf{k}} L'_{\mathbf{k}\sigma} \exp(-\mathrm{i}\mathbf{k}\cdot\mathbf{R}_{i'})$ where $i' = i + \hat{x}/2 + \hat{y}/2$.

Supplementary Note 4: Superconducting transition temperature in the three-band Hubbard model — For the 6×6 and 4×4 DCA calculations presented in the main text, the QMC Fermion sign problem prevents calculations down to temperatures low enough to determine the superconducting transition temperature T_c from the temperature where the leading eigenvalue of the Bethe-Salpeter equation crosses 1, i.e. $\lambda_d(T = T_c) = 1$. This temperature can be reached on a 2×2 cluster, however, and $T_c(n_h)$ can be determined as a function of hole density n_h in that case. Supplementary Figure **1** shows the DCA results for $T_c(n_h)$ obtained in a 2×2 cluster for the same model parameters as used in the main text. Similar to the electron-hole asymmetry found in Fig. 1 **c** for the leading eigenvalue $\lambda_d(n_h)$ of the particle-particle Bethe-Salpeter equation, as well as the asymmetry found in experiments, the T_c versus n_h phase diagram exhibits a higher maximum T_c on the hole doped side than on the electron-doped side. Moreover, these results are similar to previous DCA 2×2 cluster calculations for a similar two-band model [8], although the critical hole doping where T_c vanishes is reduced compared to those earlier calculations. This difference may originate in the difference in model parameters, in particular the neglect of the direct oxygen-oxygen hopping t_{pp} in the earlier two-band model calculations.

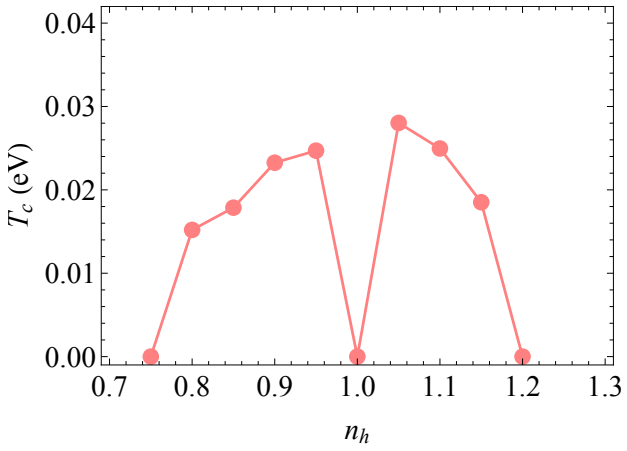

Supplementary Figure 1: **Superconducting transition temperature as a function of filling for a $N_{Cu} = 2 \times 2$ DCA cluster**. The transition temperature T_c is estimated by finding the temperature at which the leading BSE eigenvalue goes to 1. The model parameters are (in units of eV) $\Delta = 3.24$, $t_{pd} = 1.13$, $t_{pp} = 0.49$, $U_{pp} = 0$, and $U_{dd} = 8.5$. Our calculations find two superconducting domes on the hole-doped and electron-doped sides of the phase diagram, respectively, with a maximum T_c that is higher for the hole-doped case, consistent with experiments.

Supplementary Note 5: Dependence of the leading eigenfunction on temperature, cluster size and oxygen Coulomb repulsion — While the leading eigenvalue $\lambda_d(T)$ shows a very strong increase with decreasing temperature, the temperature dependence of the corresponding eigenfunction is found to be rather weak. Supplementary Figure 2 shows how the orbital and spatial structure of the leading eigenfunction $\phi_{\mathbf{r}_\beta}(\mathbf{r}_\alpha)$ of the (symmetrized) Bethe-Salpeter equation changes with decreasing temperature between $\beta = 1/T = 10$ eV^{-1} (top panels **a**-**c** from Fig. 2 in the main text) and $\beta = 12$ eV^{-1} (bottom panels **d**-**f**). We only observe small quantitative changes between these two temperatures.

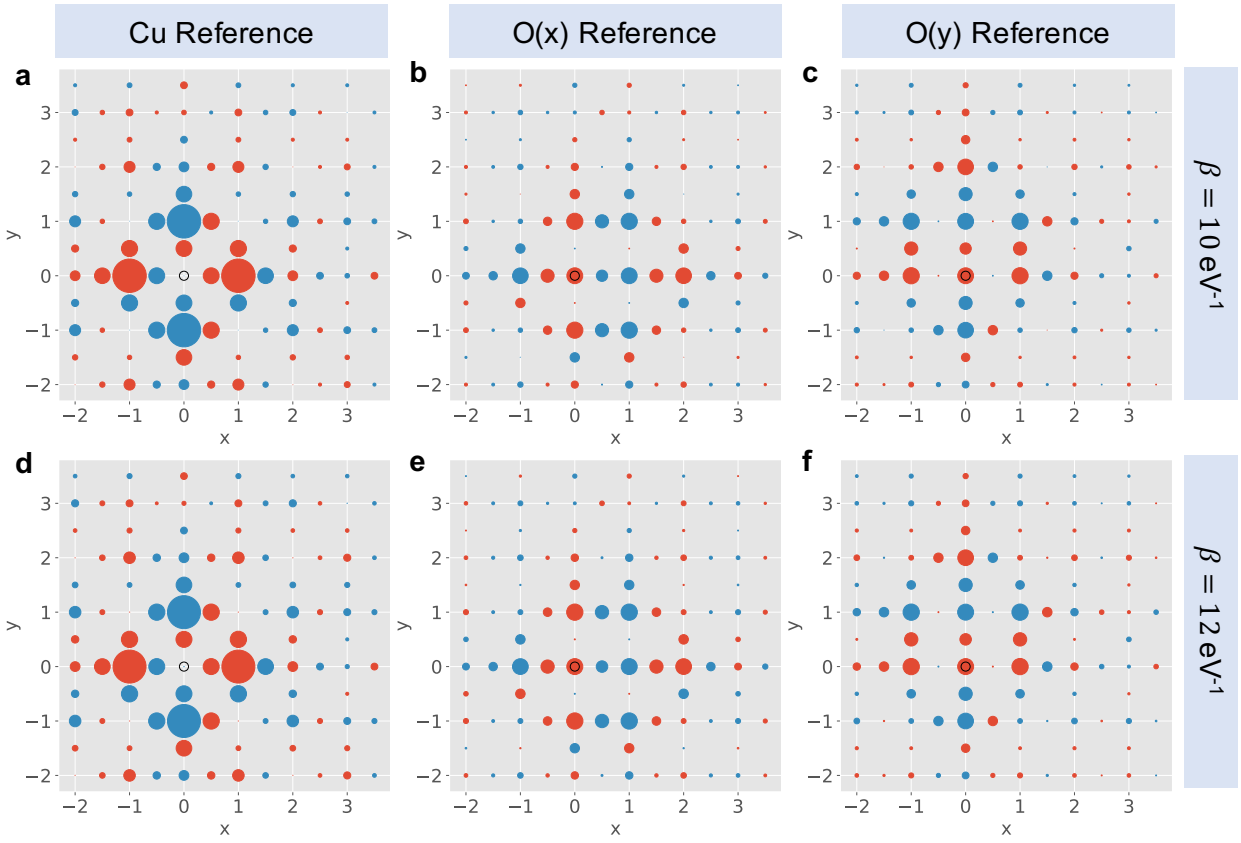

Supplementary Figure 2: **Temperature dependence of the orbital structure of the pairs in the three-band model for the CuO_2 plane**. Each panel plots the real space components of the leading (symmetrized) eigenvector of the Bethe-Salpeter equation. The top and bottom rows show results obtained on a $N_{\mathrm{Cu}} = 6 \times 6$ cluster with a hole filling $n_h = 1.15$ at an inverse temperature $\beta = 10$ eV^{-1} and $\beta = 12$ eV^{-1} respectively. The remaining model parameters are (in units of eV) $t_{pd} = 1.13$, $t_{pp} = 0.45$, $\Delta = 3.24$, $U_{pp} = 0$, and $U_{dd} = 8.5$. The left column describes the pairing between a Cu d reference site and all other orbitals as a function of distance. The middle column describes pairings with respective to a p_x orbital reference. The right column describes pairings with respective to a p_y orbital orbital reference. All panels set the Cu $3d$ orbital at the origin, as labeled by the open ring. Only slight changes are observed in the pair structure between these two temperatures.

The cluster size dependence of the leading eigenfunction is studied in Supplementary Figure 3, which shows the results of an $N_{\mathrm{Cu}} = 4 \times 4$ cluster calculation for a 15% hole doped and a 15% electron doped system. These results should be compared with Supplementary Figure 2 (or Fig. 2 in the main text), which displays the same calculation for a larger $N_{\mathrm{Cu}} = 6 \times 6$ cluster. From this comparison, one sees that the 4×4 cluster is large enough to contain the important components of the eigenfunction. Since the Fermion sign problem is much less severe in the 4×4 cluster, it allows for calculations at lower temperatures or with an additional on-site Coulomb repulsion U_{pp} on the oxygen orbitals.

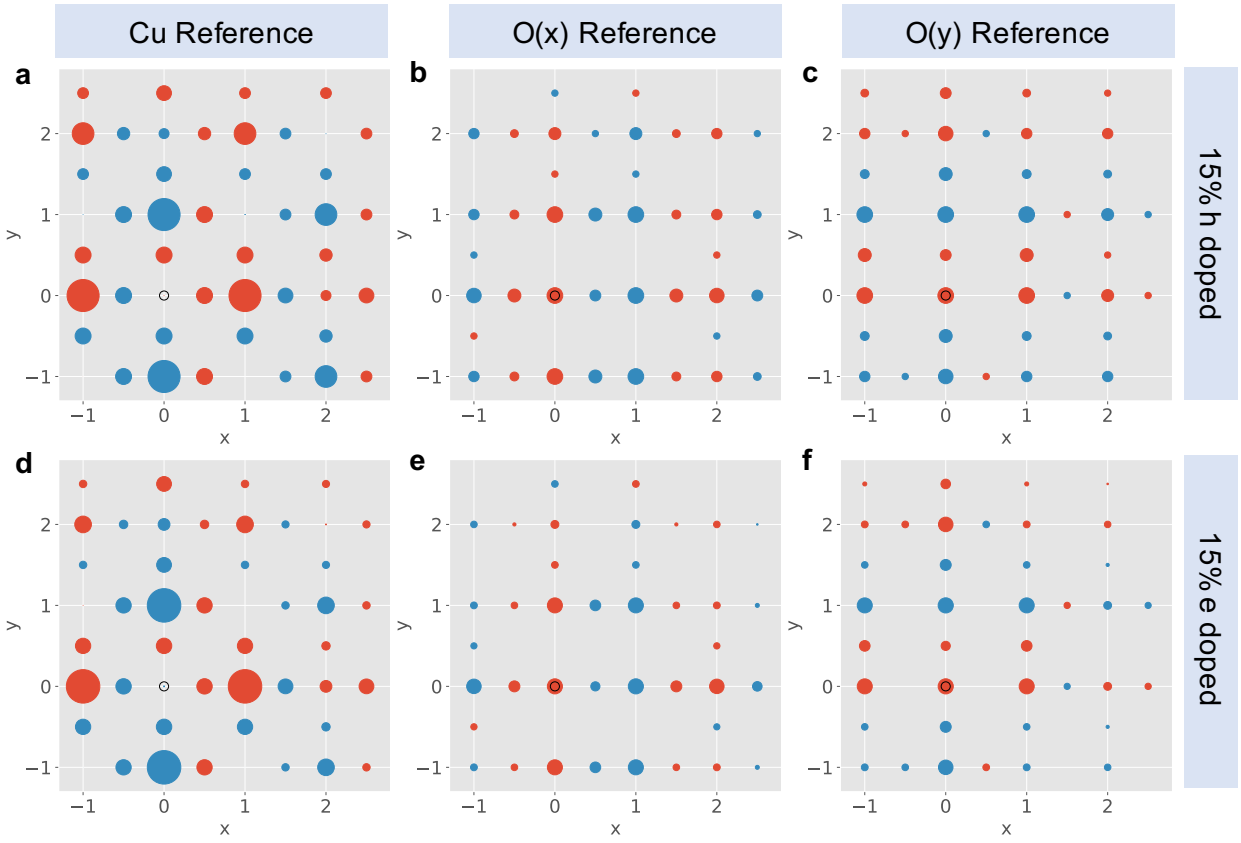

Supplementary Figure 3: **The orbital structure of the pairs in the three-orbital model for the CuO_2 plane.** Each panel plots the real space components of the leading (symmetrized) eigenvector of the Bethe-Salpeter equation. The top and bottom rows show results for hole- ($n_h = 1.15$) and electron-doping ($n_h = 0.85$), respectively, obtained on $N_{\mathrm{Cu}} = 4 \times 4$ clusters and at an inverse temperature $\beta = 16$ eV^{-1}. The remaining model parameters are (in units of eV) $t_{pd} = 1.13$, $t_{pp} = 0.45$, $\Delta = 3.24$, $U_{pp} = 0$, and $U_{dd} = 8.5$. The left column describes the pairing between a Cu d reference site and all other orbitals as a function of distance. The middle column describes pairings with respect to a p_x orbital reference. The right column describes pairings with respect to a p_y orbital orbital reference. All panels set the Cu $3d$ orbital at the origin, as labeled by the open ring. Compared with Fig. 2 in the main text, the 4×4 cluster contains the same essential pair structure as the 6×6 cluster and makes it possible to explore lower temperatures and stronger interactions.

An additional $U_{pp} = 4.1$ eV term is considered in the data for the pair structure shown in Supplementary Figure 4. Other model parameters are unchanged from those considered in Supplementary Figure 3. Comparing these images with those in Supplementary Figure 3, one sees that the structure of the eigenfunction remains almost unchanged by the additional U_{pp}. Only a very slight suppression of the components that involve the O-p orbitals is observed. This justifies the neglect of U_{pp} in most of our calculations, and provides evidence that our main conclusions reached from those calculations are general and not affected by U_{pp}.

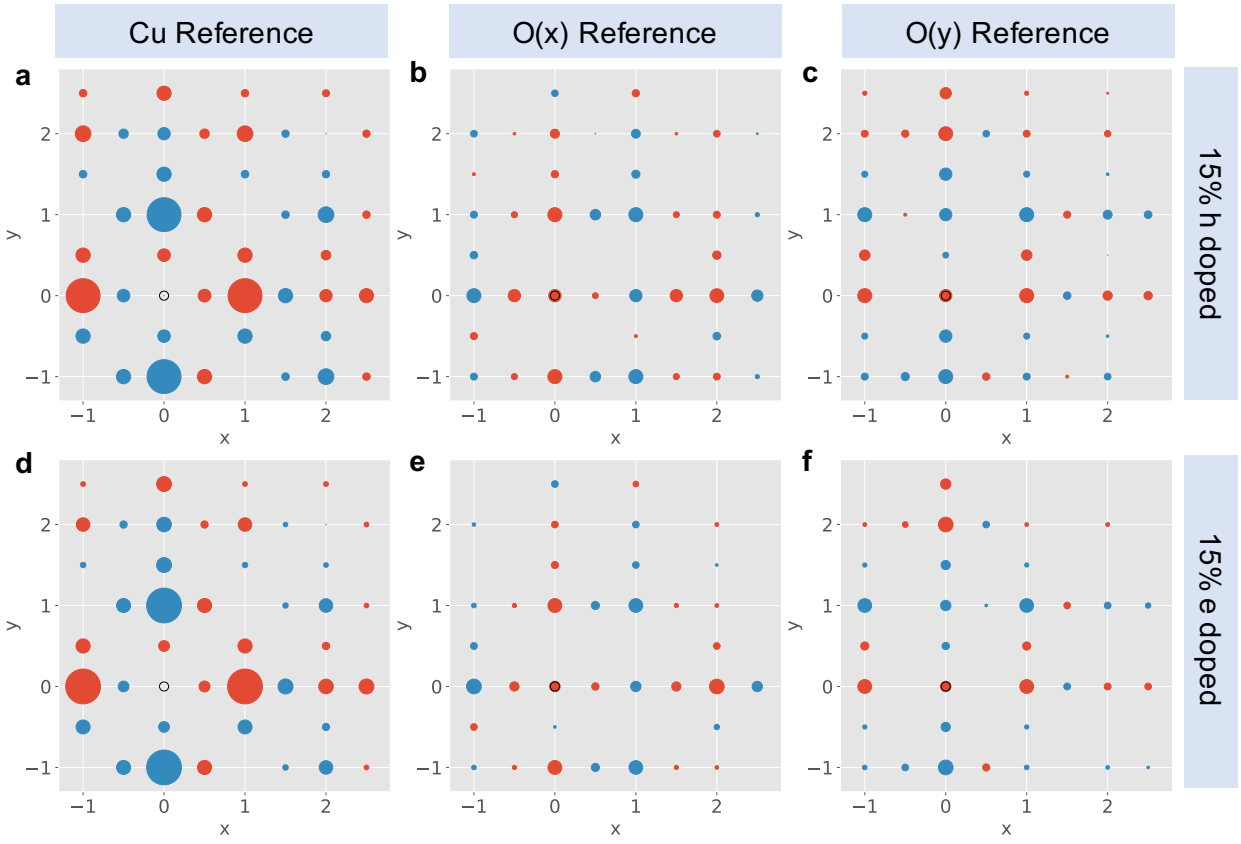

Supplementary Figure 4: **Effect of finite U_{pp} on the orbital structure of the pairs in the three-band model with finite oxygen Coulomb repulsion U_{pp}.** Each panel plots the real space components of the leading (symmetrized) eigenvector of the Bethe-Salpeter equation. The first and second rows show results for hole- ($n_h = 1.15$) and electron-doping ($n_h = 0.85$), respectively, obtained on $N_{Cu} = 4 \times 4$ clusters and at an inverse temperature of $\beta = 10$ eV^{-1} and finite $U_{pp} = 4.1$. The remaining model parameters are (in units of eV) $t_{pd} = 1.13$, $t_{pp} = 0.45$, $\Delta = 3.24$ and $U_{dd} = 8.5$. Compared to Supplementary Figure **3**, the effect of a finite U_{pp} is very weak, with only a very slight suppression of the components that involve the O-p orbitals.

Supplementary Note 6: Role of the anti-bonding molecular L′ orbital — Finally, we show the components of the leading eigenfunction that involve the antibonding L' orbital in the bottom row

of Supplementary Figure 5, compared to the bonding L components that were already shown in Fig. 3 of the main text. From the results for the orbital hole densities in Fig. 4**a** of the main text, it is clear that the L' molecular orbital remains almost completely unoccupied over the entire doping range considered, despite the finite hybridization between the L and L' states. As a consequence, and as seen from the bottom row of Supplementary Figure 5, the L' state is not involved in the pairing. This provides strong support for the Zhang-Rice picture, which only considers the d- and L-states in the mapping to an effective single-band model.

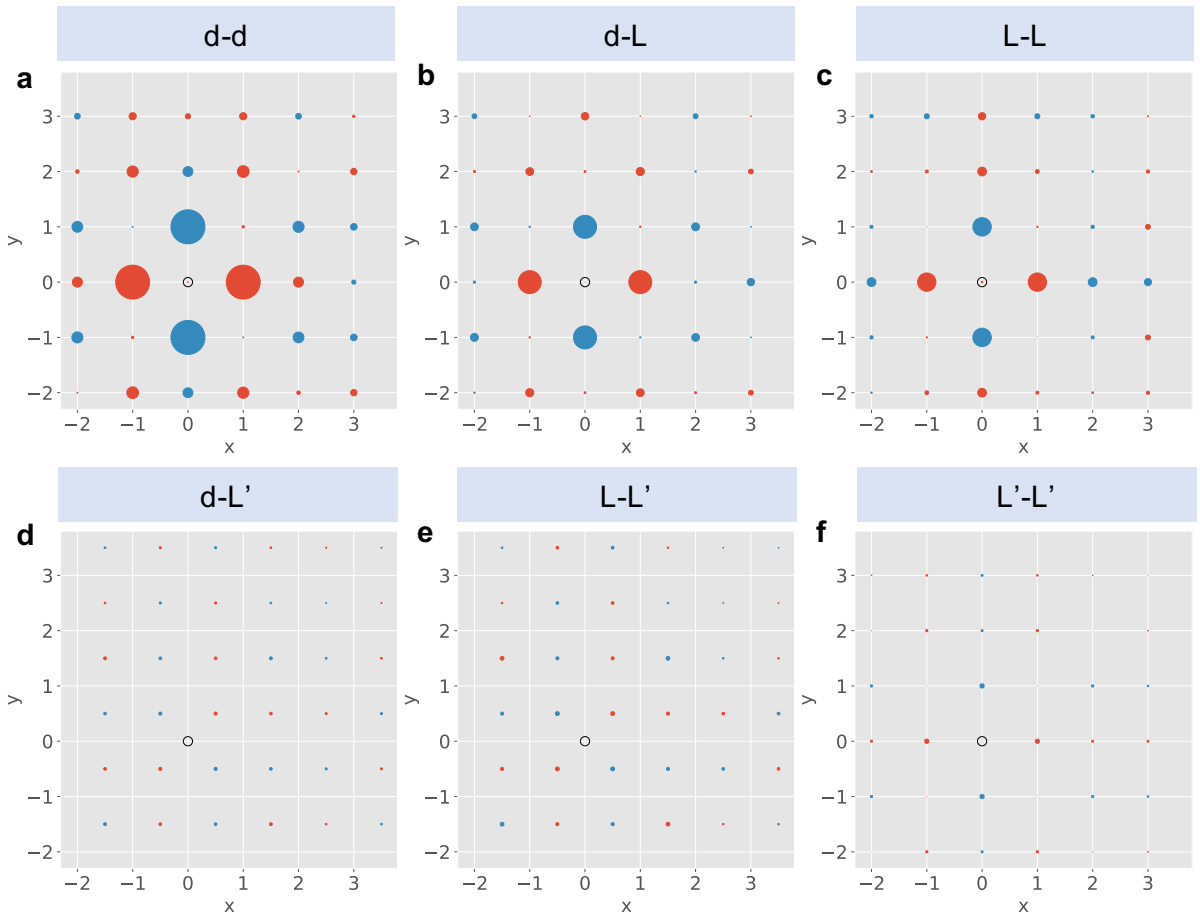

Supplementary Figure 5: **The L′-related components of the Cooper pairs in the three-band model for the CuO_2 plane.** d-L', L-L', L'-L' pairing components are presented in panel **d**, **e**, **f**, respectively, as compared with Panel **a**-**c** from Fig. 3 in the main text. All results were obtained on a $N_{Cu} = 6 \times 6$ cluster with a filling $n_h = 1.15$ and at an inverse temperature $\beta = 10$ eV^{-1}. The remaining model parameters are (in units of eV) $t_{pd} = 1.13$, $t_{pp} = 0.49$, $U_{pp} = 0$, and $U_{dd} = 8.5$. The same scale is used for the size of the points in the top and bottom rows. The pairing with the L'-orbital is negligible.

[1] Kung, Y. F. *et al.* Characterizing the three-orbital Hubbard model with determinant quantum Monte Carlo. *Phys. Rev. B* **93**, 155166 (2016).

[2] Czyżyk M. T. & Sawatzky, G. A. Local-density functional and on-site correlations: The electronic structure of La_2CuO_4 and $LaCuO_3$. *Phys. Rev. B* 49, 14211 (1994).

[3] Johnston, S., Vernay, F. & Devereaux, T. Impact of an oxygen dopant in $Bi_2Sr_2CaCu_2O_8$. *Eur. phys. Lett.* **86**, 37007 (2009).

[4] Ohta, Y., Tohyama, T. & Maekawa, S. Apex oxygen and critical temperature in copper oxide superconductors: Universal correlation with the stability of local singlets. *Phys. Rev. B* **43**, 2968 (1991).

[5] Zhang, F. C. & Rice, T. M. Effective Hamiltonian for the superconducting Cu oxides. *Phys. Rev. B* **37**, 3759(R) (1988).

[6] Zölfl, M. B., Maier, T. A., Pruschke, T. & Keller, J. Electronic properties of CuO_2-planes: A DMFT study. *Eur. Phys. J. B* **13**, 47 (2000).

[7] Avella, A., Mancini, F., Mancini, F. P. & Plekhanov, E. Emery vs. Hubbard model for cuprate superconductors: a composite operator method study. *Eur. Phys. J. B* **86**, 265 (2013).

[8] Macridin, A., Jarrell, M., Maier, T. A. & Sawatzky, G. A. Physics of cuprates with the two-band Hubbard model: The validity of the one-band Hubbard model. *Phys. Rev. B* **71**, 134527 (2005).